INTERNATIONAL JOURNAL FOR NUMERICAL METHODS IN FLUIDS, VOL. 19, 527–548 (1994)

# UPSTREAM MONOTONIC INTERPOLATION FOR SCALAR TRANSPORT WITH APPLICATION TO COMPLEX TURBULENT FLOWS

F. S. LIEN AND M. A. LESCHZINER

*Department of Mechanical Engineering, University of Manchester Institute of Science and Technology (UMIST), Manchester M60 1QD, U.K.*

## SUMMARY

A new monotonic scheme for the approximation of steady scalar transport is formulated and implemented within a collocated finite-volume/pressure-correction algorithm for general turbulent flows in complex geometries. The scheme is essentially a monotonic implementation of the quadratic QUICK interpolation and uses a continuous and compact limiter to secure monotonicity. The principal purpose is to allow an accurate and fully bounded, hence stable, approximation of turbulence convection in the context of two-equation eddy viscosity and Reynolds stress transport modelling of two- and three-dimensional flows, both subsonic and transonic. Among other benefits, this capability permits an assessment to be made of the adequacy of approximating turbulence convection with first-order upwind schemes in conjunction with higher-order formulations for mean-flow properties—a widespread practice. The performance characteristics of the bounded scheme are illustrated by reference to computations for scalar transport, for a transonic flow in a Laval nozzle, for one separated laminar flow and for two separated turbulent flows computed with a non-linear RNG model and full Reynolds stress closure.

KEY WORDS Monotonic interpolation TVD MUSCL Turbulence transport Modelling Numerical accuracy

## 1. INTRODUCTION

The accuracy with which transport processes are approximated numerically is of crucial importance in assessing the predictive realism of mathematical models which represent physical processes, particularly those associated with turbulence in high-Reynolds-number and high-Mach-number flows. Advection usually poses the biggest problems, since this process provokes or is associated with steep property gradients and thus raises the need for high-accuracy approximation schemes.

Because advection is represented by a first-order derivative, its approximation by a first-order numerical scheme can be argued to be both appropriate and consistent on physical as well as mathematical grounds. Indeed, the essential validity of this argument is reflected, among others, by the unconditional boundedness of the first-order upwind scheme, due to the absence of parasitic components in the resulting numerical solution. However, this scheme is generally unacceptable on grounds of accuracy, unless extremely fine grids are used, since it introduces a high level of artificial second-order diffusion which tends to seriously erode property gradients in the same way as physical diffusion does.

The use of higher-order approximations is the route most frequently taken in efforts to increase accuracy. However, schemes of order two and above, particularly symmetric ones, can provoke

CCC 0271–2091/94/180527–22 *Received November 1993*

spurious oscillations when the Peclet number is high in combination with steep gradients of the flow properties. Such oscillations are not merely *optical defects* but can have seriously deleterious or even catastrophic effects on the iterative stability and convergence properties of coupled systems. This is particularly the case when transport equations are solved for turbulence quantities, such as turbulence energy, its rate of dissipation or normal Reynolds stresses, for which negative values arising from oscillations can lead to negative diffusive transport and hence instability.

The tendency towards oscillation may be counteracted, in principle, by adding to an oscillatory scheme a component which introduces a bias towards upstream flow conditions or strengthens the bias which may already be an inherent feature of the scheme. This can be effected either explicitly, by the addition of an artificial diffusion fragment to the advective flux returned by the basic scheme (e.g. Jameson *et al.*[1]), or implicitly, through an increase in the contribution or weight of values residing at the upstream nodes of the approximation stencil (e.g. Warming and Beam[2]). If, as is usually the case, the strength of the oscillation-damping mechanism is decided upon by an *a priori* choice of weighting factors or coefficients, then the resulting composite scheme will not, in general, be monotonic. To achieve monotonicity, upstream biasing must be controlled by the oscillatory features of the solution, i.e. the scheme must be non-linear.

Early proposals for using non-linear limiters, sensitized to the ratio of consecutive gradients of the numerical solution, were made by Boris and Book[3,4] and van Leer.[5–7] It was not until 1983, however, that Harten[8] injected formal mathematical rigour into the subject by proposing the *total variation diminishing* (TVD) concept as the criterion for developing high-resolution convection schemes which combine accuracy with monotonicity and entropy preservation. The rationale is quite simple, in principle, and has been stated by reference to general conservation laws by Sweby[9] as follows:

> *Given a basic scheme which preserves second-order accuracy in space and time, but which is unbounded, an appropriate limiter is introduced which diminishes the oscillation-provoking, antidiffusive truncation error on the basis of the TVD constraint.*

Within the framework of an explicit time-marching solution, any second-order-accurate TVD scheme, both in time and space, may be constructed by linearly blending the Lax–Wendroff[10] and Warming–Beam[2] schemes in conjunction with a 'smart' slope limiter which switches off the antidiffusive flux when a local extremum (an oscillation) is detected. Different schemes arise through different limiter forms and Sweby[9] has presented a general framework, in terms of a TVD diagram, which encompasses a wide range of limiters, including those of van Leer,[5] Chakravarthy and Osher[11] and Roe.[12] If, on the other hand, interest is focused on the steady state only, it is possible to re-interpret Sweby's TVD diagram in terms of the *normalized variable diagram* (NVD) proposed by Leonard.[13] Using this NV diagram and following Sweby's rationale, Leonard[13] and Gaskell and Lau[14] have formulated the SHARP and SMART schemes, respectively, both being monotonic implementations of Leonard's third-order QUICK scheme.[15] In essence, both formulations switch between QUICK and lower-order schemes depending upon the local value of the ratio of gradients used to identify the presence of an extremum. Algorithmically, both schemes involve the use of several conditional statements which give rise to high computational expense, particularly on vector machines. Tamamidis and Assanis[16] reported, for example, that the CPU time required by SHARP exceeded that needed by QUICK by a factor of 6·5 when both were applied to a simple scalar transport problem on a 100 × 100 grid.

In this paper, a continuous and highly compact QUICK-based limiter is proposed and implemented within a general non-orthogonal finite-volume algorithm[17] for calculating 2D and 3D turbulent incompressible and compressible flows. The scheme typically requires only 20% more CPU time than QUICK. The performance of the limiter—identified by the acronym

UMIST (Upstream Monotonic Interpolation for Scalar Transport)—is examined by reference to solutions for several flow problems, including scalar advection, transonic inviscid flow, one separated laminar flow and two separated turbulent flows, one behind a backward-facing step and the other over a high-lift aerofoil. In the last two flows, turbulence is modelled either by a non-linear eddy-viscosity form[18] of the RNG model[19] or by the second-moment closure of Gibson and Launder.[20] The use of such complex models in the present context reflects the authors' principal interest in turbulence modelling of multidimensional separated flows. Hence, the thrust of the present numerical effort is directed towards securing uniformly high accuracy, iterative stability and efficiency for all equations solved within a Reynolds-averaged procedure which incorporates the most general turbulence closures available.

One specific advantage of the capability arising from the above combination is that the benefits derived from approximating turbulence convection accurately in complex conditions can be investigated. It is generally assumed that the solution of these equations is rather insensitive to convection because of the strong dominance of source-like terms. This assumption has been widely used as a justification for approximating turbulence convection with first-order schemes in combination with higher-order approximations for mean-flow convection.

## 2. MATHEMATICAL FORMULATION

### *2.1. Basic TVD concepts*

The construction of any numerical scheme required to be monotonicity-preserving rests on two general principles.

1. No new local extrema must be created.
2. The value of an existing local minimum must be non-decreasing and that of a local maximum must be non-increasing.

These principles can be described formally by defining the *total variation* (TV) of a set of discrete data $\phi_i$ such as that shown in Figure 1 ($i = 1$ to 5):

$$\mathrm{TV}(\phi) \equiv |\phi_2 - \phi_1| + |\phi_3 - \phi_2| + |\phi_4 - \phi_3| + |\phi_5 - \phi_4| = |\phi_3 - \phi_1| + |\phi_3 - \phi_5|. \quad (1)$$

For monotonicity to be satisfied, this total variation must not increase.

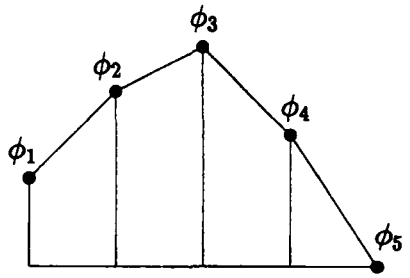


$$\mathrm{TV}(\phi) \equiv |\phi_2 - \phi_1| + |\phi_3 - \phi_2| + |\phi_4 - \phi_3| + |\phi_5 - \phi_4|$$
$$= |\phi_3 - \phi_1| + |\phi_3 - \phi_5|$$

Figure 1. Example of discrete data set illustrating TV property

Consider the spatially one-dimensional scalar conservation law

$$\frac{\partial \phi}{\partial t} + a \frac{\partial \phi}{\partial x} = 0, \quad a > 0. \tag{2}$$

The solution is said to be TVD[8] if

$$\mathrm{TV}(\phi^{n+1}) \leqslant \mathrm{TV}(\phi^n). \tag{3}$$

A general discrete approximation of the conservation law (2) is

$$\phi_i^{n+1} = \phi_i^n - C_{i-1/2}\Delta_{i-1/2}\phi^n + D_{i+1/2}\Delta_{i+1/2}\phi^n, \tag{4}$$

in which $\Delta$ is the central-difference operator and $C$ and $D$ are scheme-specific 'influence coefficients'. In terms of form (4), conditions sufficient to secure inequality (3) are

$$C_{i+1/2} \geqslant 0, \qquad D_{i+1/2} \geqslant 0, \qquad C_{i+1/2} + D_{i+1/2} \leqslant 1. \tag{5}$$

Any time-marching scheme approximating the convective transport of a scalar property $\phi$ may generally be written as the sum of a diffusive first-order upwind term and a diffusion-compensating 'antidiffusive' term, the latter designed to achieve high accuracy:

$$\phi^{n+1} = \phi^n - \underbrace{v\Delta_{i-1/2}\phi^n}_{\text{first-order upwinding}} - \underbrace{\frac{v(1-v)}{2}\left(\frac{\varphi(r_{i+1/2})}{r_{i+1/2}} - \varphi(r_{i-1/2})\right)\Delta_{i-1/2}\phi^n}_{\text{antidiffusive flux}} \tag{6}$$

where

$$v = a\Delta t/\Delta x, \qquad r_{i+1/2} = \Delta_{i-1/2}\phi^n/\Delta_{i+1/2}\phi^n. \tag{7}$$

The choice of $\varphi(r)$ dictates the order of the scheme and its boundedness properties. Second-order accuracy may, for example, be attained by the choice

$$\varphi(r) = (1-\alpha)\underbrace{1}_{\text{L-W}} + \alpha\underbrace{r}_{\text{W-B}}, \quad 0 \leqslant \alpha \leqslant 1, \tag{8}$$

which represents a weighted linear average of the Lax–Wendroff scheme[10] ('1') and the Warming–Beam scheme[2] ('$r$'). While this approximation is not unconditionally bounded (TVD), Sweby[9] has shown that a TVD form arises from the constraint

$$\varphi(r) = \min(2r, 2), \quad r > 0, \qquad \varphi(r) = 0, \quad r \leqslant 0. \tag{9}$$

Hence, any form of equation (6) for which $\varphi(r)$ lies in the shaded area of Figure 2 is bounded. A particularly advantageous route through the shaded region of Figure 2, identified by the bold line, is described by Sweby's '$\Phi$-limiter'

$$\varphi(r)_\Phi = \max[0, \min(\Phi r, 1), \min(r, \Phi)], \tag{10}$$

where $1 \leqslant \Phi \leqslant 2$. For $\Phi = 1$, $\varphi(r)_\Phi$ can be described by the 'minmod' function, i.e. $\varphi(r)_\Phi = \mathrm{minmod}(1, r)$, with minmod defined as

$$\mathrm{minmod}(x, y) = \mathrm{sgn}(x)\max[0, \min(|x|, \mathrm{sgn}(x)y)]. \tag{11}$$

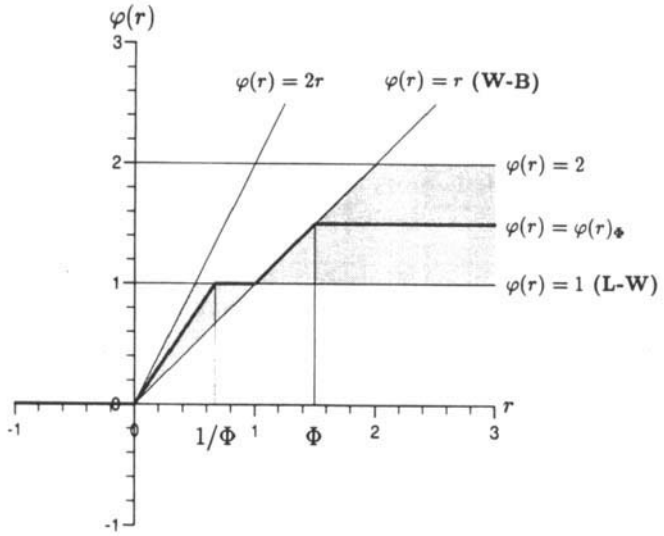


Figure 2. Range of boundedness-preserving limiter for monotonic blend of Lax–Wendroff and Warming–Beam schemes

For $\Phi = 2$, the 'superbee' limiter of Roe[12] is recovered. This particular form of (10) obeys the symmetry condition:

$$\varphi(r) = r\varphi(1/r), \tag{12}$$

which ensures that the forward and backward gradients are treated in the same manner—a useful condition, as will transpire later.

### 2.2. *The MUSCL approach*

In the context of an iterative solution for statistically steady flows within the finite-volume framework, the essential task is to approximate the volume-face fluxes, combining accuracy with boundedness. For a one-dimensional 'volume' and positive velocity, schemes of up to third-order accuracy may be constructed by approximating, say, the face value $\phi_f$ in Figure 3 by the upwind

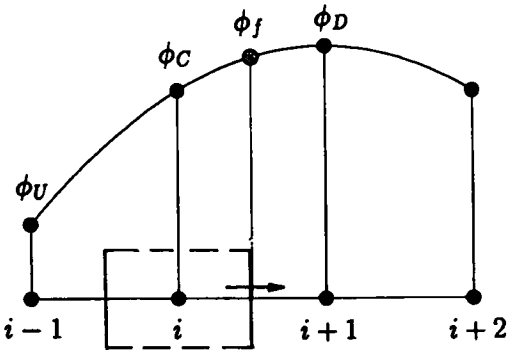


Figure 3. One-dimensional finite volume and associated nodal stencil used to formulate MUSCL limiter for face 'f'

value $\phi_U$ corrected by an 'antidiffusive' gradient involving $\phi_D$, $\phi_C$ and $\phi_U$. This is one key feature of van Leer's MUSCL scheme. A general form of such a scheme may be written as

$$\phi_f = \phi_C + \tfrac{1}{4}[(1+\kappa)(\phi_D - \phi_C) + (1-\kappa)(\phi_C - \phi_U)], \tag{13}$$

where the numerical parameter '$\kappa$' controls the order of the scheme. Unbounded forms corresponding to central differencing (CD), second-order (linear) upwind differencing (LUDS) and Leonard's quadratic upstream-weighted differencing (QUICK) arise by setting $\kappa = 1$, $-1$ and 0·5 respectively.

The approach to constructing bounded forms leans on that outlined in Section 2.1. Thus, to render equation (13) monotonic, whilst retaining a five-point stencil (for 1D), a slope limiter $\varphi(r_f)$ is introduced in a manner analogous to that in equation (6):

$$\phi_f = \phi_C + \tfrac{1}{4}[(1+\kappa)\varphi(r_f)(\phi_D - \phi_C) + (1-\kappa)\varphi(1/r_f)(\phi_C - \phi_U)]. \tag{14}$$

For further consideration it is expedient to replace the dimensional convected property $\phi$ by the normalized variable $\tilde{\phi}$ defined as[13]

$$\tilde{\phi} = \frac{\phi - \phi_U}{\phi_D - \phi_U}. \tag{15}$$

With this definition equation (14) may be written as

$$\tilde{\phi}_f = \tilde{\phi}_C + \tfrac{1}{4}[(1+\kappa)\varphi(r_f)(1 - \tilde{\phi}_C) + (1-\kappa)\varphi(1/r_f)\tilde{\phi}_C]. \tag{16}$$

Since

$$r_f = \frac{\tilde{\phi}_C}{1 - \tilde{\phi}_C}, \tag{17}$$

equation (16) may be simplified to

$$\tilde{\phi}_f = \tilde{\phi}_C + \tfrac{1}{4}[(1+\kappa)\varphi(r_f) + (1-\kappa)r_f\varphi(1/r_f)](1 - \tilde{\phi}_C). \tag{18}$$

If, next, a *symmetric limiter* satisfying condition (12) is chosen, then equation (18) becomes

$$\tilde{\phi}_f = \tilde{\phi}_C + \frac{\varphi(r_f)}{2}(1 - \tilde{\phi}_C), \tag{19}$$

which is evidently independent of the parameter $\kappa$. Substitution of equation (17) into equation (9) allows the TVD constraints to be expressed as

$$\begin{gathered} \tilde{\phi}_f \leqslant 1, \quad \tilde{\phi}_f \leqslant 2\tilde{\phi}_C, \quad \tilde{\phi}_f \geqslant \tilde{\phi}_C, \quad \text{for } 0 < \tilde{\phi}_C < 1, \\ \tilde{\phi}_f = \tilde{\phi}_C \quad \text{for } \tilde{\phi}_C \leqslant 0 \text{ or } \tilde{\phi}_C \geqslant 1. \end{gathered} \tag{20}$$

It will be recalled that Sweby's TVD condition, taken in conjunction with the Lax–Wendroff/Warming–Beam blend, was represented by the shaded area in Figure 2. An analogous graphical representation can readily be derived using condition (20) together with form (13), the latter written for the special case of a weighted linear average of the central-differencing scheme ($\kappa = 1$) and the second-order upwind scheme ($\kappa = -1$), i.e.

$$\tilde{\phi}_f = (1-\alpha)\underbrace{\tfrac{1}{2}(1 + \tilde{\phi}_C)}_{\text{CD}} + \underbrace{\alpha\,\tfrac{3}{2}\tilde{\phi}_C}_{\text{LUDS}}, \quad 0 \leqslant \alpha \leqslant 1. \tag{21}$$

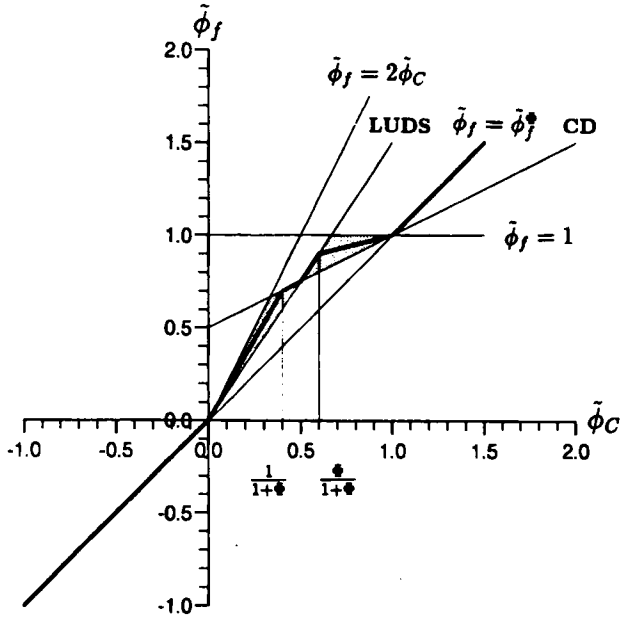


Figure 4. Sweby's Φ-limiter within NV diagram

This graphical representation is given in Figure 4, and the shaded area is again the range in which the composite second-order scheme is fully bounded. Moreover, the bold line in Figure 4 represents Sweby's 'Φ-limiter' as given by equation (10).

### 2.3. *The UMIST limiter*

By far the most popular higher-order convection scheme used for turbulent-flow calculations is the QUICK approximation of Leonard,[15] which for a uniform grid is third-order accurate. While this scheme is upstream-biased, it is not bounded, giving rise to oscillations at Peclet numbers higher than $Pe = 2$. A monotonic version of QUICK satisfying the constraints (9) and (20) may be achieved through the limiter

$$\varphi(r) = \max[0, \min(2r, \underbrace{0{\cdot}75 + 0{\cdot}25r}_{\text{QUICK}}, 2)]. \tag{22}$$

This limiter is not symmetric, however, and a simplification to the form (19), with consequent reduction in the number of arithmetic operations, is not possible. An alternative *symmetric* limiter form is

$$\varphi(r) = \max[0, \min(2r, 0{\cdot}25, +\, 0{\cdot}75r, \underbrace{0{\cdot}75 + 0{\cdot}25r}_{\text{QUICK}}, 2)], \tag{23}$$

which in terms of equation (19) is equivalent to

$$\tilde{\phi}_f = \tilde{\phi}_C + 0{\cdot}5 \max\left[0, \min\left(\frac{2\tilde{\phi}_C}{1-\tilde{\phi}_C}, 0{\cdot}25 + \frac{0{\cdot}75\tilde{\phi}_C}{1-\tilde{\phi}_C}, \underbrace{0{\cdot}75 + \frac{0{\cdot}25\tilde{\phi}_C}{1-\tilde{\phi}_C}}_{\text{QUICK}}, 2\right)\right](1-\tilde{\phi}_C). \tag{24}$$

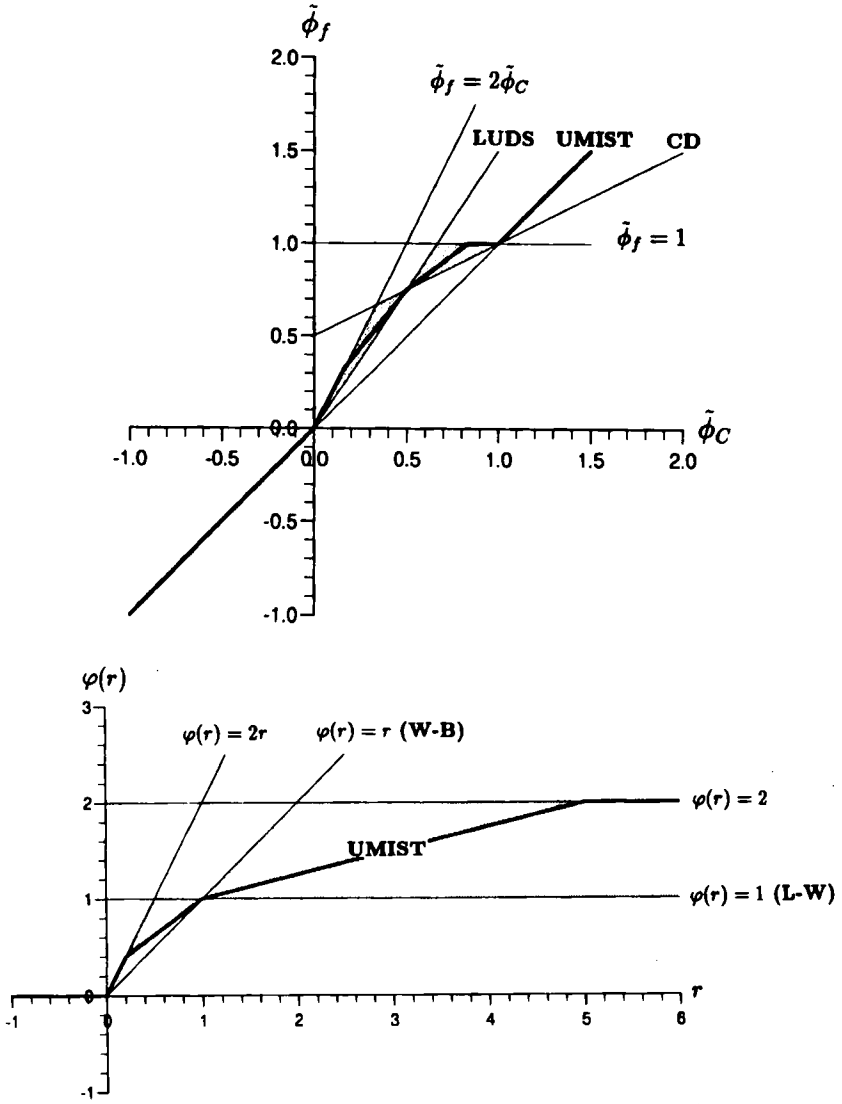


Figure 5. UMIST limiter within TVD and NV diagrams

This is termed here the UMIST limiter. The TVD and NV diagrams corresponding to equations (23) and (24) are shown in Figure 5.

### *2.4. Multidimensional implementation*

The partial differential equations governing the transport of any scalar quantity $\phi$ can be written in terms of tensor notation applicable to the general co-ordinate system $\xi_j$ as

$$\frac{\partial}{\partial \xi^j}\left[U^j \rho \phi - \Gamma_\phi J\left(q^{jn}_{mm}\frac{\partial \phi}{\partial \xi^n}\right)\right] = JS_\phi. \tag{25}$$

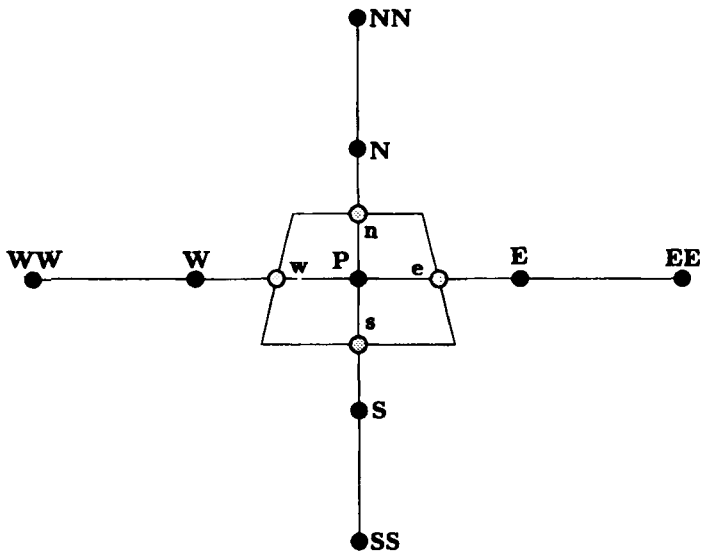


Figure 6. Two-dimensional non-orthogonal finite volume and stencil used for implementation of UMIST limiter

Here the Jacobian matrix $J$, the contravariant velocity vector $U^j$ and the fourth-order tensor $q^{jn}_{mi}$ are given, respectively, by

$$J = \frac{\partial(x, y, z)}{\partial(\xi, \eta, \zeta)}, \qquad U^j = J\beta^j_m u^m, \qquad q^{jn}_{mi} = \beta^j_m \beta^n_i, \tag{26}$$

where $\beta^j_m$ are the elements of the inverse Jacobian matrix $J^{-1}$.

To simplify the following consideration without loss of generality, it is expedient to focus on the 2D situation only. The 3D extension is quite straightforward and introduces no novel aspects. Intergration of equation (25) over the finite volume shown in Figure 6 and application of the Gauss divergence theorem in conjunction with central differencing for diffusion yields a balance of the face fluxes and volume-integrated net source. The face values of $\phi$ are approximated by the first-order upwind scheme in conjunction with an appropriate antidiffusive flux implemented via a 'deferred correction' source term $S^{DC}_{\phi}$ which is controlled by the UMIST limiter. Finally, the sources are discretized via a single-point quadrature and linearized as

$$JS_{\phi} = S_P\phi_P + S_C, \tag{27}$$

with $S_P$ being so chosen as to be unconditionally negative. Insertion of the above approximation into the volume-integrated equation gives

$$A_P\phi_P = \sum_{m=E,W,N,S} A_m\phi_m + S_C + S^{DC}_{\phi}, \tag{28}$$

where

$$A_E = \left(\Gamma_\phi \frac{x_\eta^2 + y_\eta^2}{J}\right)_e - \max[(\rho U)_e, 0], \qquad A_W = \left(\Gamma_\phi \frac{x_\eta^2 + y_\eta^2}{J}\right)_w + \max[(\rho U)_w, 0],$$
$$A_N = \left(\Gamma_\phi \frac{x_\xi^2 + y_\xi^2}{J}\right)_n - \max[(\rho V)_n, 0], \qquad A_S = \left(\Gamma_\phi \frac{x_\xi^2 + y_\xi^2}{J}\right)_s + \max[(\rho V)_s, 0], \tag{29}$$
$$A_P = A_E + A_W + A_N + A_S - S_P$$

and

$$U = uy_\eta - vx_\eta, \qquad V = vx_\xi - uy_\xi. \tag{30}$$

The source term $S_\phi^{DC}$ pertaining to the deferred correction is given by

$$S_\phi^{DC} = 0{\cdot}5\{[(\rho U)_e^+ \varphi(r_e^+) - (\rho U)_e^- \varphi(r_e^-)](\phi_E - \phi_P) + [(\rho U)_w^+ \varphi(r_w^+) - (\rho U)_w^- \varphi(r_w^-)](\phi_P - \phi_W)$$
$$+ [(\rho V)_n^+ \varphi(r_n^+) - (\rho V)_n^- \varphi(r_n^-)](\phi_N - \phi_P) + [(\rho V)_s^+ \varphi(r_s^+) - (\rho V)_s^- \varphi(r_s^-)](\phi_P - \phi_S)\}, \tag{31}$$

in which $\varphi(r)$ is defined as in (24),

$$(\rho U)^\pm = \frac{\rho U \pm |\rho U|}{2}, \qquad (\rho V)^\pm = \frac{\rho V \pm |\rho V|}{2} \tag{32}$$

and

$$r_e^+ = \frac{\phi_P - \phi_W}{\phi_E - \phi_P}, \quad r_e^- = \frac{\phi_E - \phi_{EE}}{\phi_P - \phi_E}, \quad r_w^+ = \frac{\phi_W - \phi_{WW}}{\phi_P - \phi_W}, \quad r_w^- = \frac{\phi_P - \phi_E}{\phi_W - \phi_P},$$
$$r_n^+ = \frac{\phi_P - \phi_S}{\phi_N - \phi_P}, \quad r_n^- = \frac{\phi_N - \phi_{NN}}{\phi_P - \phi_N}, \quad r_s^+ = \frac{\phi_S - \phi_{SS}}{\phi_P - \phi_S}, \quad r_s^- = \frac{\phi_P - \phi_N}{\phi_S - \phi_P}. \tag{33}$$

## 3. NUMERICAL FRAMEWORK

The approximation scheme outlined in Section 2 has been implemented within the general flow algorithm 'STREAM'.[17] The procedure is applicable to two- and three-dimensional flows, using a non-orthogonal, fully collocated, structured finite-volume arrangement. In its standard mode of operation the procedure iterates the solution towards a steady state by means of a pressure-correction algorithm for all Mach numbers, including transonic conditions. Turbulence is represented optionally by way of linear and non-linear, standard and RNG $k$–$\varepsilon$ model variants or full second-moment closure. Various hybrid approaches have been realized and tested, including such combining Reynolds-stress closure in the inner field with low-Reynolds-number $k$–$\varepsilon$ models in the semi-viscous near-wall region, both under 2D and 3D conditions.

In one application to follow, the flow is transonic and thus described by a mixed hyperbolic/elliptic conservation law. For this particular case the UMIST limiter has been incorporated into a cell-centred, explicit time-marching scheme which determines the density and mass flux in a point-coupled fashion by using the characteristic variables; the latter arise upon diagonalization of the Jacobian coefficient matrix premultiplying the flux vector in the convection term.[21]

## 4. APPLICATIONS

### *4.1. Overview of test cases*

In order to convey a broad view of the characteristics of the scheme documented in Section 2.3, computational results are included here for the following five test cases:

(i) inviscid flow in a 1D Laval nozzle;
(ii) convective and diffusive transport of a scalar property by a rotational velocity field[22];
(iii) laminar flow through axisymmetric stenosis[23];
(iv) turbulent flow past a backward-facing step with the upper wall inclined at 6°[24];
(v) turbulent flow over the ONERA-A aerofoil at 13·3° incidence.[25]

The application of a 'minmod' limiter similar to UMIST to further cases, among them a three-dimensional turbulent flow in a circular-sectioned bend, is documented in Reference 26.

It ought to be pointed out that the main intention of the present study is to identify the sensitivity of predictions to the choice of the convection scheme, particularly that applied to the turbulence equations in the fourth and fifth cases above. Therefore, physical issues, in particular the influence of turbulence-model variants in conjunction with different near-wall treatments, are not addressed in detail. The predictive performance of a range of turbulence models for the cases considered herein is examined in other papers.[27,28]

### *4.2. Inviscid flow in a Laval nozzle*

This first application is intended to convey the capabilities of the UMIST limiter in the geometrically and physically simple but numerically demanding case of a normal shock provoked in a convergent–divergent nozzle by an elevated back pressure acting on a supersonic flow. Conventional linear schemes usually rely on explicit diffusive fluxes or an implicit dissipative mechanism when required to resolve this discontinuity, and these almost invariably give rise either to excessive shock smearing or to oscillatory features at the edges of the shock. Here the principal challenge posed to any limiter is to reduce the dissipative contribution to the lowest possible level while eliminating artificial extrema.

The area variation of the Laval nozzle chosen here is given by

$$\begin{aligned} A(x) &= A_{tr} + (A_i - A_{tr})[(5 - x)/5]^2, \quad 0 \leqslant x \leqslant 5, \\ A(x) &= A_{tr} + (A_o - A_{tr})[(5 - x)/5]^2, \quad 5 \leqslant x \leqslant 10, \end{aligned} \tag{34}$$

where $A_i$, $A_{tr}$ and $A_o$ denote the cross-sectional areas at inlet, throat and outlet respectively. The area ratio $A_i{:}A_{tr}{:}A_o$ has been selected as 2:1:2 and the exit pressure has been prescribed to be 0·65 times the stagnation pressure, implying a normal shock at the position $x = 0{\cdot}9$.

As explained briefly in Section 3, the numerical approach adopted here is different from that of other cases because of the mixed hyperbolic/elliptic nature of the conservation law. Thus the equations governing continuity and momentum were solved for density and mass flux in a point-coupled fashion and in terms of characteristic variables within a time-marching cell-centred scheme. A consequence of this approach is that the TVD condition is only strictly satisfied for the 'locally frozen' conservation law in which the 'coefficients' multiplying the vector of characteristic variables remain invariant during the forward time step.[21]

Figure 7 compares distributions for Mach number and pressure, calculated using 100 nodes, with corresponding analytical solutions derived from 1D theory. As seen, the shock is very well resolved within two internodal intervals without any hint of oscillation.

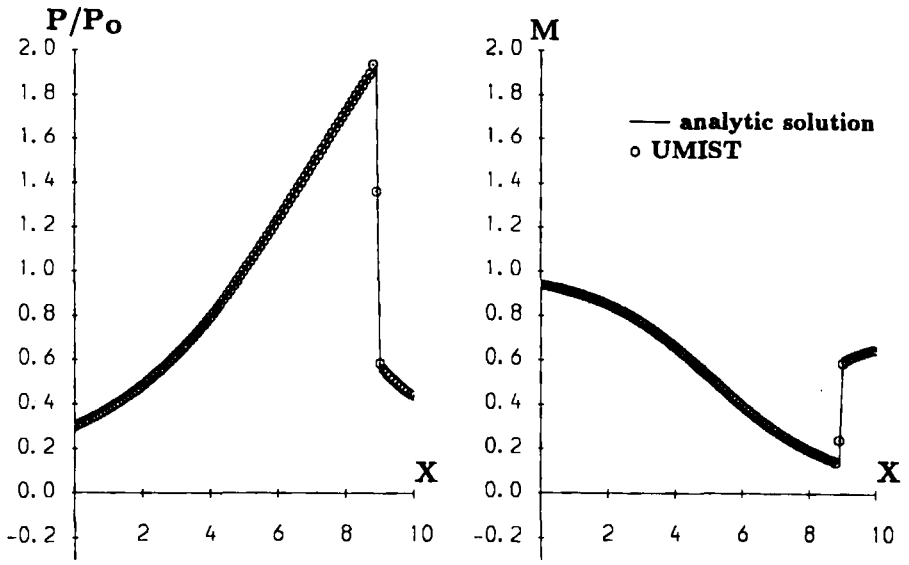


Figure 7. Transonic Laval nozzle flow—pressure and Mach number variations

### *4.3. Scalar advection by a rotational velocity field*

The convective/diffusive transport of a scalar step across a Cartesian mesh by a rotational motion is a searching test of the quality of any convection scheme, particularly one formulated on the basis of one-dimensional considerations but applied to multidimensional transport. This is the issue on which the present application focuses.

In terms of Cartesian co-ordinates the steady transport of a scalar in two-dimensional space is governed by the equation

$$\frac{\partial u\phi}{\partial x} + \frac{\partial v\phi}{\partial y} = \frac{1}{P_e}\left(\frac{\partial^2\phi}{\partial x^2} + \frac{\partial^2\phi}{\partial y^2}\right) \quad \text{for } -1 \leqslant x \leqslant 1, 0 \leqslant y \leqslant 1. \tag{35}$$

The particular test conditions chosen here are identical to those used in a test problem which was the focus of an IAHR workshop on convection schemes organized by Smith and Hutton[22] in 1982. These may be written as

$$u = 2y(1 - x^2), \qquad v = -2x(1 - y^2), \tag{36}$$

with boundary conditions pertaining to (35) of

$$\begin{aligned} \phi &= 1 - \tanh(10) \quad \text{for } x = 1, 0 \leqslant y \leqslant 1, \\ \phi &= 1 - \tanh(10) \quad \text{for } x = -1, 0 \leqslant y \leqslant 1, \\ \phi &= 1 - \tanh(10) \quad \text{for } y = 1, -1 \leqslant x \leqslant 1, \\ \phi &= 1 + \tanh[10(2x + 1)] \quad \text{for } y = 0, -1 \leqslant x \leqslant 0, \\ \partial\phi/\partial y &= 0 \quad \text{for } y = 0, 0 \leqslant x \leqslant 1, \end{aligned} \tag{37}$$

for which $\phi$ becomes 0 at $x = \pm 1$ and nearly 2 at the origin. Solutions have been obtained over a 40 × 20 grid for two Peclet numbers, namely 500 and $10^6$. For the former value the diffusive

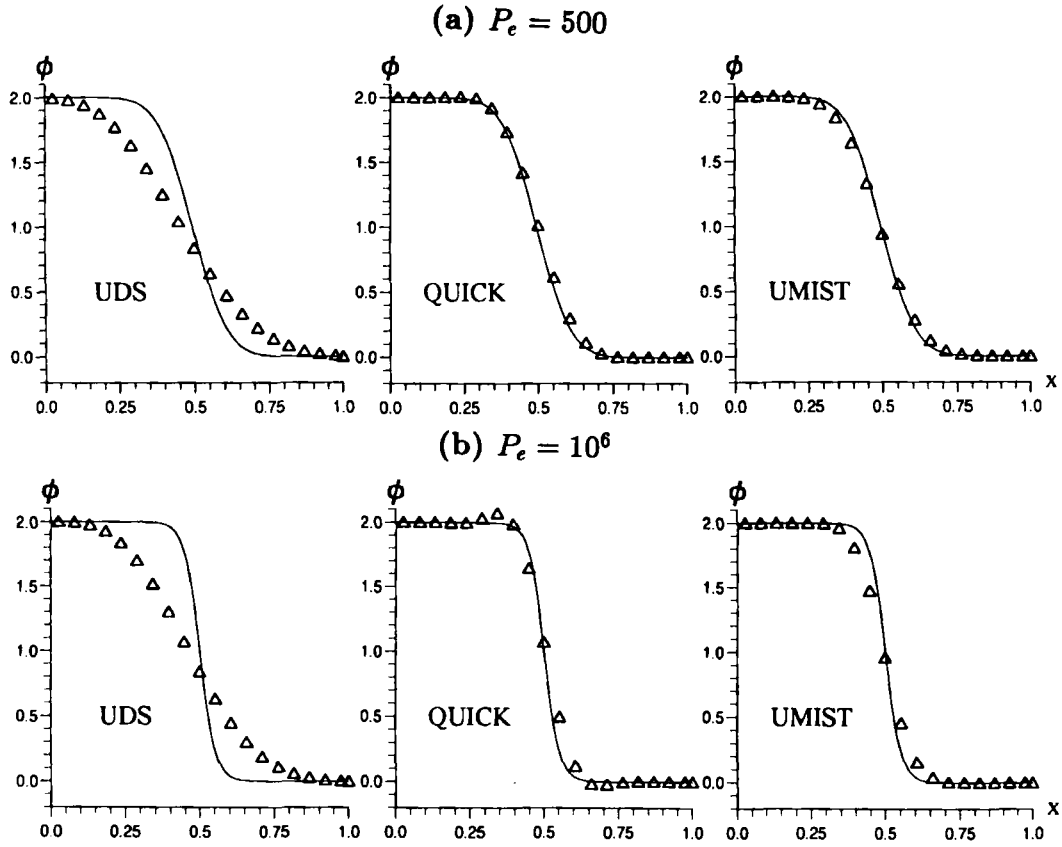


Figure 8. Scalar transport by rotational velocity field—profiles of scalar property after 180° rotation

process is relatively weak but still influential, while for the latter diffusion is negligible. Since there is no analytical solution in the presence of diffusion, reference solutions have been obtained with the UMIST limiter over a fine $300 \times 150$ grid and are assumed to represent the exact solutions against which coarse-grid solutions may be contrasted when the accuracy of alternative schemes are assessed.

Solutions for $\phi$ obtained with the first-order upwind scheme UDS, the quadratic scheme QUICK and the UMIST limiter are shown in Figures 8(a) and 8(b) for $Pe = 500$ and $10^6$ respectively. In the case of $Pe = 500$, UMIST yields results very close to QUICK. However, at $Pe = 10^6$, QUICK provokes under- and overshoots close to the region of steep $\phi$-variation, $x = 0{\cdot}5$. In contrast, UMIST returns a fully bounded solution, which indicates, however, that this has been achieved at the penalty of some smoothing at the lower and upper edges of the scalar step. The first-order upwind scheme UDS clearly returns an unacceptable erosion of the scalar gradients due to a high level of second-order diffusion provoked by the leading truncation error of this scheme. Similar conclusions can be drawn from the contour plots of $\phi$ shown in Figures 9(a) and 9(b) for $Pe = 500$ and $10^6$ respectively.

A comparison of CPU times required for the fine-grid computation is given in Table I. As seen, the overheads associated with the implementation of the UMIST limiter are very modest, being of the order of 15% higher than the execution times required for QUICK. These overheads

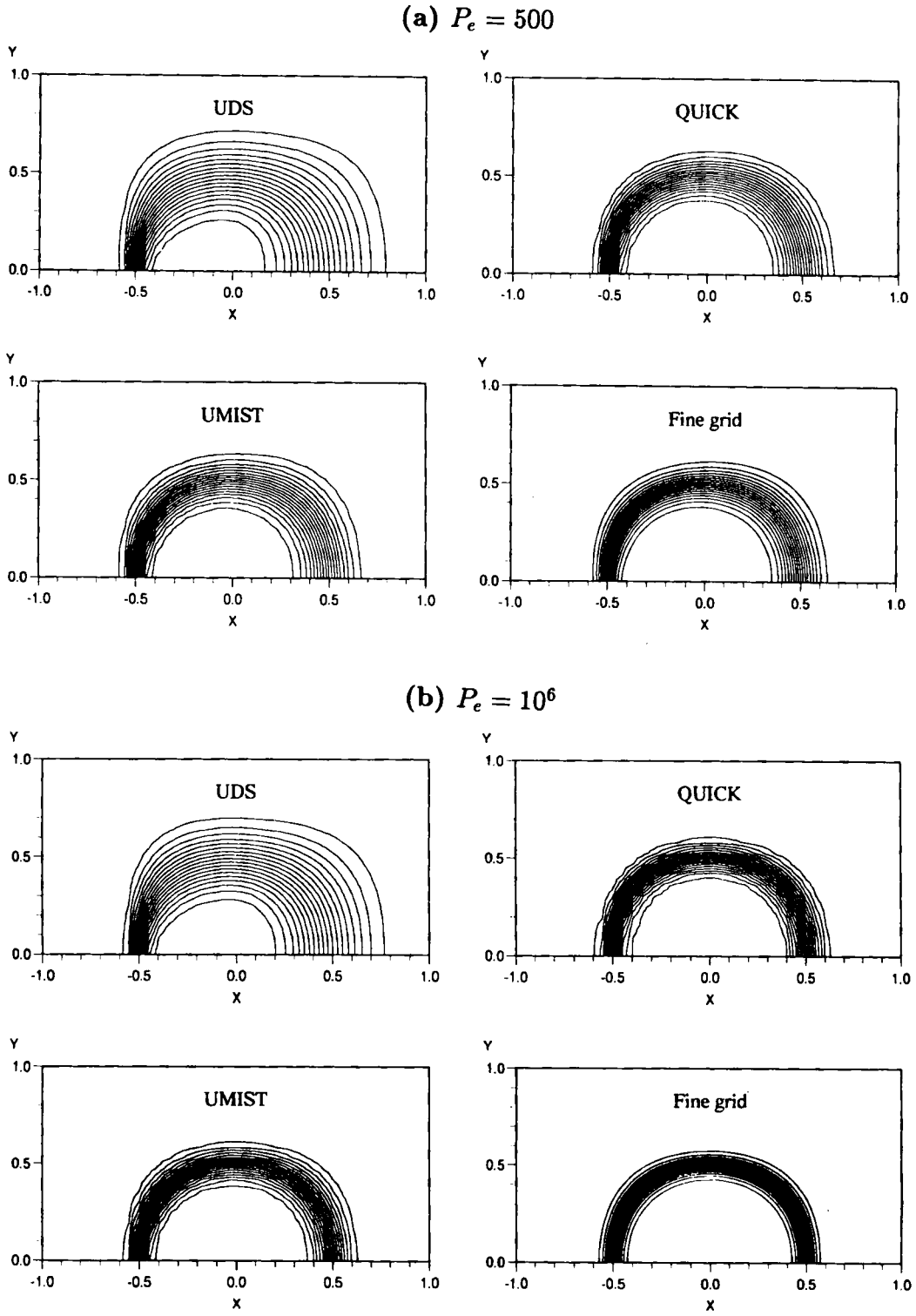


Figure 9. Scalar transport by rotational velocity field—contour plots of scalar property

Table I. Relative resource requirements of alternative convection schemes

| Convection scheme | Iterations | CPU time(s) | Seconds per iteration | CPU ratio |
|---|---|---|---|---|
| | | $Pe = 500$ | | |
| UDS | 202 | 29·967 | 0·1484 | 1·000 |
| QUICK | 196 | 32·862 | 0·1677 | 1·130 |
| UMIST | 196 | 37·827 | 0·1930 | 1·301 |
| | | $Pe = 10^6$ | | |
| UDS | 95 | 13·997 | 0·1473 | 1·000 |
| QUICK | 89 | 15·010 | 0·1687 | 1·072 |
| UMIST | 89 | 17·364 | 0·1950 | 1·241 |

are mainly attributable to the evaluation of the intrinsic MAX and MIN functions which are used by the limiter.

### 4.4. *Laminar flow through axisymmetric stenosis*

While monotonic schemes are particularly advantageous when resolving very steep gradients such as shocks, scalar jumps and strong variations in turbulent quantities provoked by high rates of strains, they can also offer benefits in resolving the momentum field, particularly in elliptic flows in which shear layers are often highly skewed relative to the mesh lines. This case is intended to illustrate the performance of UMIST in a separated flow in which significant numerical errors can easily arise in the curved shear layer bordering a recirculation bubble.

The geometry considered here is a sinusoidal constriction in a circular pipe, the radius of which is described by

$$r_{\text{wall}} = R\left\{1 - \frac{\delta}{2R}\left[1 + \cos\left(\frac{\pi x}{2R}\right)\right]\right\}, \quad -2 \leqslant \frac{x}{R} \leqslant 2, \tag{38}$$

where $R = 0{\cdot}945$ cm and $\delta = 2R/3$. Calculations have been performed for $Re_R = 98$ with a grid consisting of 70 × 30 lines. The same three schemes used for the previous test case have been used here too, with attention being focused on the sensitivity of the length and shape of the recirculation bubble to the numerical approximation.

Solutions for the streamfunction contours are shown in Figure 10. It is seen that the reattachment positions returned by QUICK and its UMIST-limited variant are virtually identical and close to the experimental location reported by Young and Tsai.[23] Under laminar flow conditions the sensitivity of predicted flow features to the order of the convection scheme is often weak, but evidently this is not the case here, as is seen from the solution obtained with the upwind scheme, because of the relatively high Reynolds number. As a consequence the cell Peclet number is high and the contribution of artificial diffusion, which is controlled by the Peclet number, is strong. This sensitivity is of considerable importance in this case, since it implies that the closeness of the QUICK and UMIST solutions is a fair reflection of the quality of UMIST, particularly in respect of the low level of artificial diffusion it introduces as part of the limiting process.

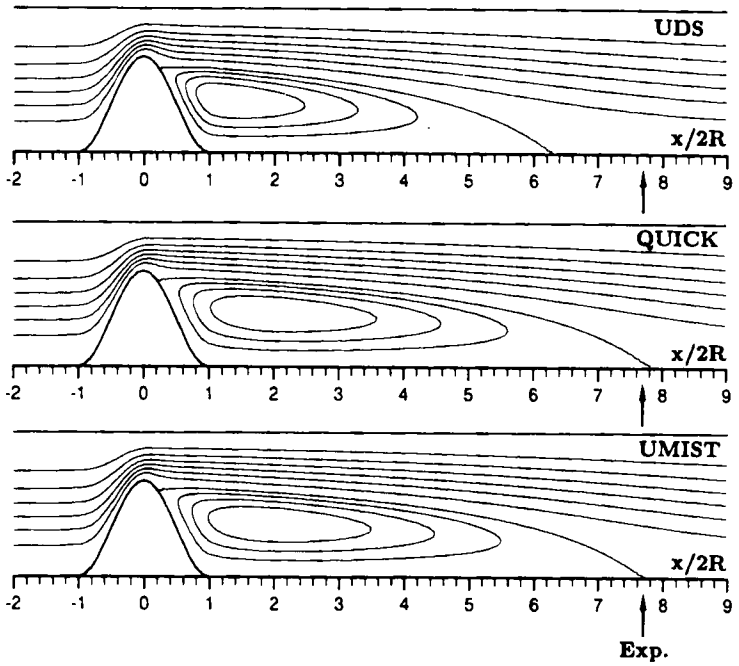


Figure 10. Laminar flow behind a pipe stenosis—contour plots of streamfunction

### *4.5. Turbulent flow over a backward-facing step*

The authors' main interest is in computing complex turbulent flows with high-accuracy schemes, and it is particularly with the view to such computations that the UMIST limiter was formulated. The case considered herein is one of two turbulent flows in which the UMIST limiter has been used specifically to examine the sensitivity of the predicted solutions to the accuracy with which the convective transport of turbulence quantities is approximated.

The geometry considered is a backward-facing step preceded by a parallel channel and followed by a diverging passage with the upper wall inclined at 6°. The particular turbulence model adopted is a combination of the RNG $k$–$\varepsilon$ model of Yakhot *et al.*[19] and the non-linear eddy-viscosity formulation of Speziale,[18] the latter with the convective fragments of the so-called Oldroyd derivative neglected. This hybrid model is applicable to high-$Re$ conditions only and has thus been implemented here in conjunction with log-law-based wall laws. This particular choice has been partly motivated by the outcome of a broader study on the performance of a range of modelling practices,[27] which has shown that the present hybrid formulation yields mean-flow solutions which are close to those derived from much more elaborate second-moment closure.

Results have been obtained with three numerical implementations. In one, both mean-flow and turbulence convection have been approximated with the upwind scheme; this variant is denoted by UDS + UDS. In the second, identified by QUICK + UDS, mean-flow convection was approximated with QUICK while turbulence convection was represented by the upwind scheme. Finally, in the third variant, QUICK for mean-flow convection was applied in conjunction with UMIST for turbulence quantities, a combination denoted by QUICK + UMIST.

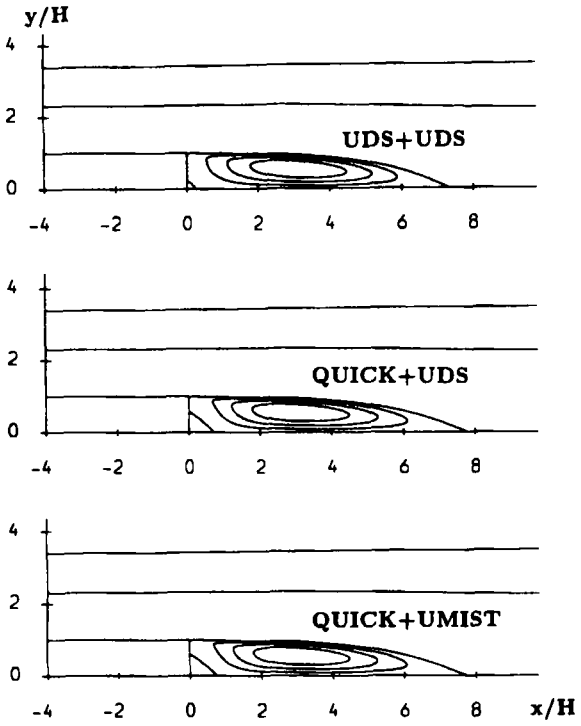


Figure 11. Turbulent flow behind a backward-facing step in 6° channel—contour plots of streamfunction

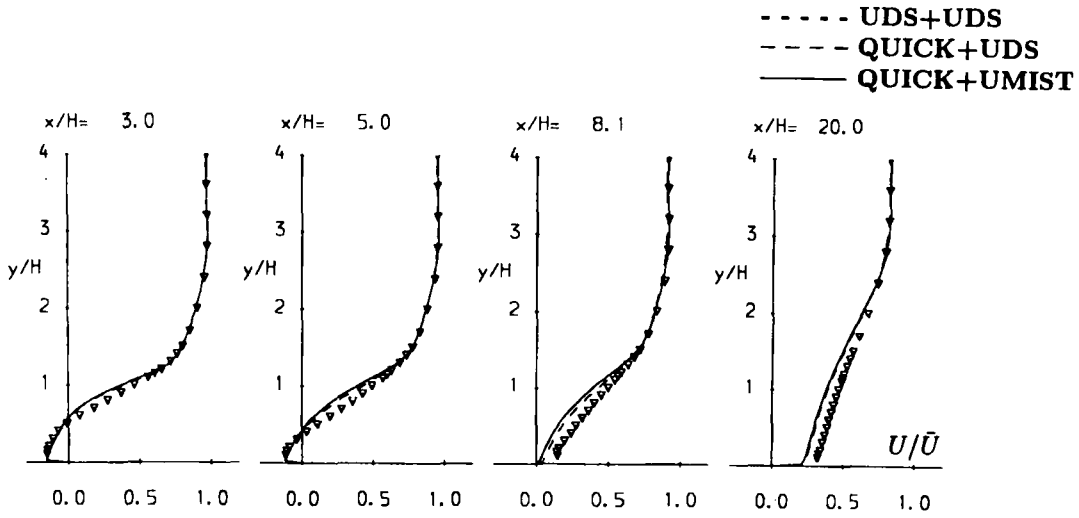


Figure 12. Turbulent flow behind a backward-facing step in 6° channel—velocity profiles

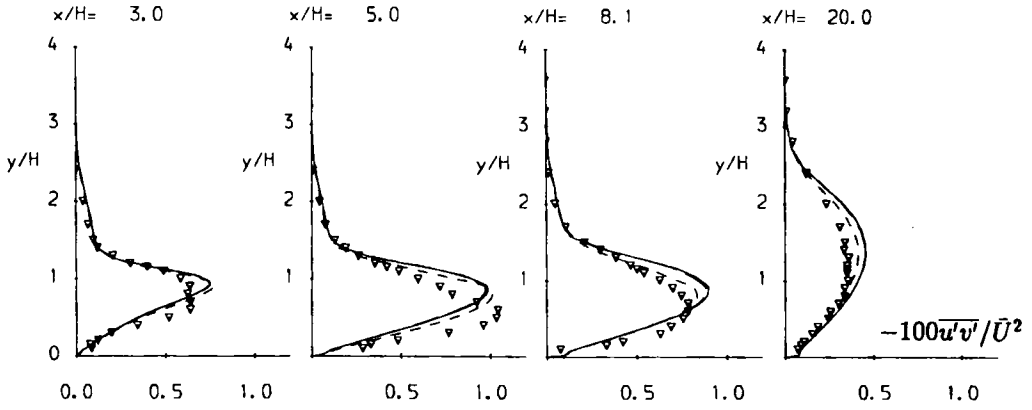


Figure 13. Turbulent flow behind a backward-facing step in 6° channel—shear stress profiles

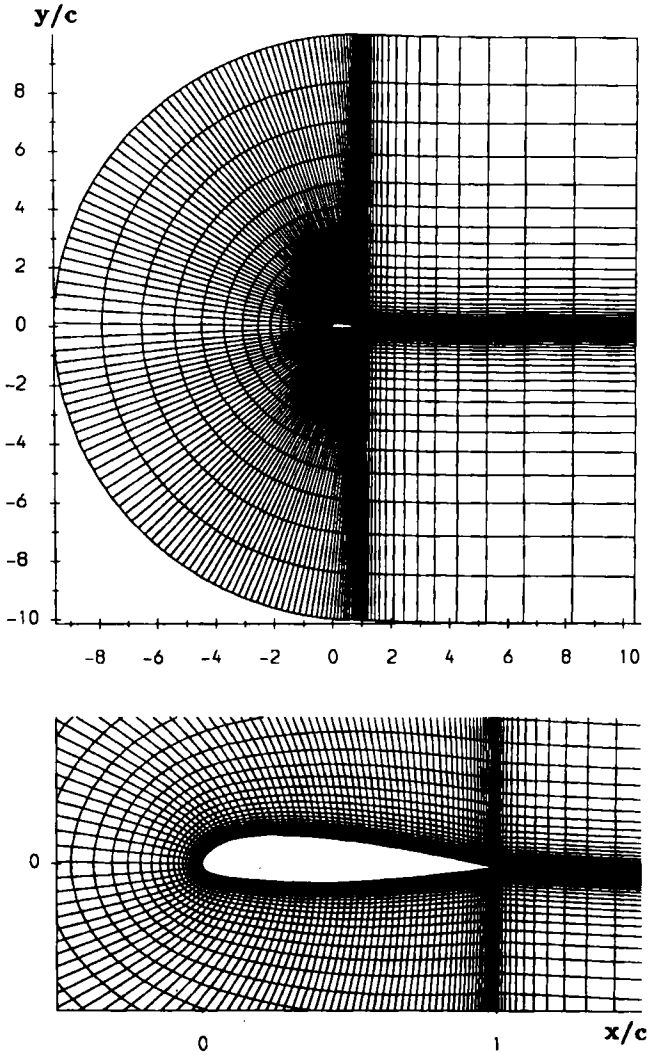


Figure 14. ONERA-A aerofoil—geometry and grid

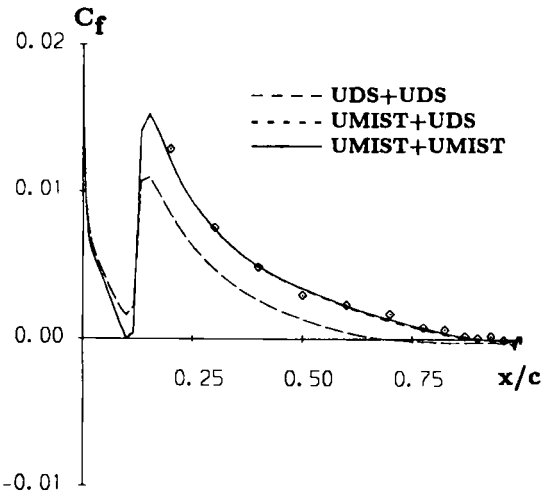


Figure 15. Flow around ONERA-A aerofoil—skin friction distribution on suction side

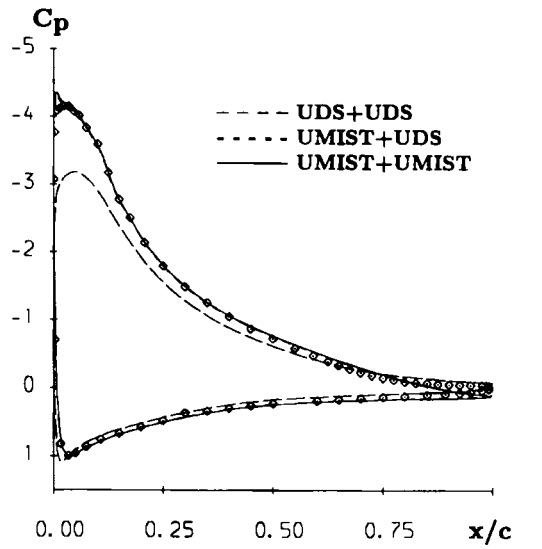


Figure 16. Flow around ONERA-A aerofoil—distribution of pressure coefficient along aerofoil surface

Considered first are the streamfunction contours shown in Figure 11. The experimental value of the reattachment point is at $x/H = 8{\cdot}2$. As seen from the plotted contours, the solutions obtained with the QUICK + UDS and QUICK + UMIST combinations are virtually identical, with the reattachment point being in good agreement with the experimental observation. Similarly, differences between corresponding velocity profiles (Figure 12) and shear-stress profiles (Figure 13) are small. This result implies that the contribution of turbulence transport to the balance of processes dictating the level of turbulence is modest, in which case the numerical approximation of this process is of marginal importance. While this is consonant with the established view that turbulence processes are largely dictated by a balance between generative

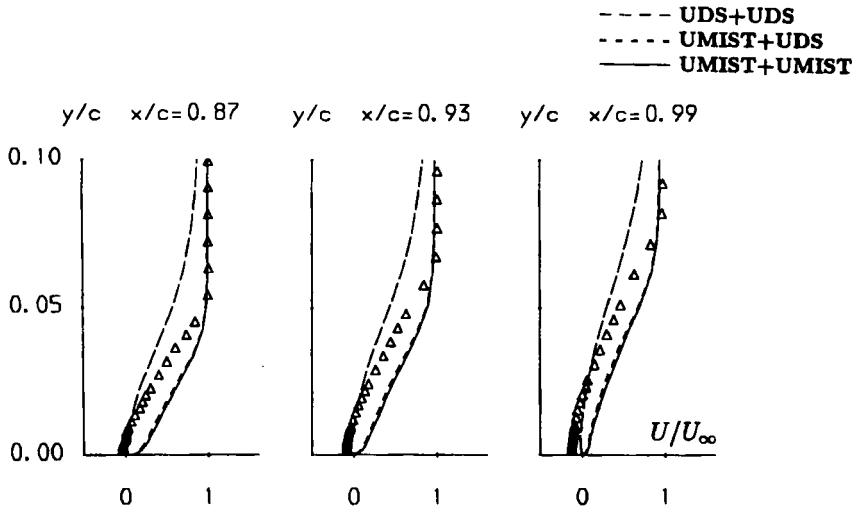


Figure 17. Flow around ONERA-A aerofoil—velocity profiles

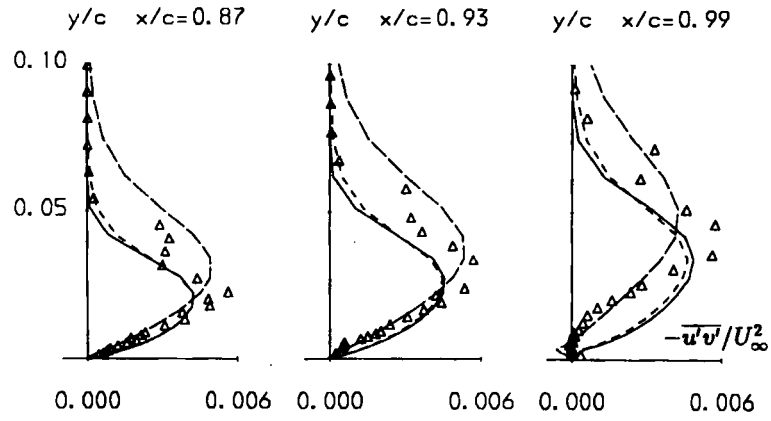


Figure 18. Flow around ONERA-A aerofoil—shear stress profiles

and destructive mechanisms, there are circumstances in which turbulence transport dominates. For example, Lien and Leschziner,[26] using a limiter somewhat cruder than UMIST, reported an elevated sensitivity to turbulence convection in a 3D circular-sectioned bend in which secondary circulation gives rise to a high level of transverse convection of turbulence energy. Figures 11–13 also show, in agreement with observations made in the previous laminar case, that the solution is very sensitive to the approximation of mean-flow convection. Here too the recirculation length is smaller, the consequence being a more rapid momentum recovery in the wake region and corresponding differences in the velocity and stress variations.

### *4.6. Turbulent flow around the ONERA-A aerofoil*

This fifth and final case is of much greater complexity than the previous flow in terms of both geometric complexity and mathematical elaboration in the turbulence closure. The aerofoil, at

13·3° incidence, is shown in Figure 14 together with the 178 × 66 C-mesh surrounding it. The calculations reported below have been made with the high-*Re* Reynolds-stress transport closure of Gibson and Launder[20] in conjunction with the one-equation $k$–$l$ low-*Re* model of Wolfshtein,[29] the latter applied to the semi-viscous near-wall region.

Solutions for skin friction, wall pressure, velocity and shear stress, obtained with different combinations of UDS, QUICK and UMIST for mean-flow and turbulence convection, are shown in Figures 15–18 respectively. A discussion of physical issues, contrasting the performance of two second-moment-closure variants with that of several eddy-viscosity models, may be found in Reference 28. Consistently with previous observations, the results bring out here again with stark clarity the importance of using a non-diffusive scheme for mean-flow convection. The use of UMIST for the convection of Reynolds stresses and turbulence dissipation, whilst permitting uniformly high accuracy to be maintained across all variables without deleterious consequences to stability, has only a marginal effect on the solution. Again, this reflects the relatively weak contribution of transport to the balance of processes in the stress equations—a fact reflected by the small differences observed in many plane 2D flows between differential and algebraic forms of second-moment closure.

## 5. CONCLUSIONS

A monotonic and compact second-order scheme based on the quadratic convection approximation QUICK has been formulated and applied to a range of test cases, among them turbulent flows modelled with advanced closure practices. The scheme can be easily incorporated into any non-monotonic framework and secures accuracy and stability regardless of the nature of the transport equation solved. The outcome of the present study may be summarized as follows.

1. The UMIST limiter returns, in most circumstances, solutions which are close to those of QUICK but without oscillatory features. This applies in particular to laminar flow conditions. Some smoothing is observed for scalar transport at very high Peclet numbers. Shocks are captured very crisply and without any oscillations.
2. In turbulent flows, the UMIST limiter allows a problem-free higher-order discretization of turbulence convection to be achieved.
3. In the turbulent cases examined, the approximation of turbulence convection is not, however, of material importance to the accuracy of the solutions.
4. In contrast, the order of approximation of momentum and scalar transport is crucial.
5. The resource overheads of UMIST are very low, of the order of 15% above those required for the non-monotonic QUICK approximation.

## REFERENCES

1. A. Jameson, W. Schmidt and E. Turkel, 'Numerical simulation of the Euler equations by finite volume methods using Runge–Kutta time-stepping schemes, *AIAA Paper 81-1259*, 1981.
2. R. F. Warming and R. M. Beam, 'Upwind second order difference schemes and applications in aerodynamics', *AIAA J.*, **14**, 1241 (1976).
3. J. P. Boris and D. L. Book, 'Flux corrected transport: I. SHASTA, a fluid transport algorithm that works', *J. Comput. Phys.*, **11**, 38 (1973).
4. J. P. Boris and D. L. Book, 'Solution of the continuity equation by the method of flux corrected transport', *J. Comput. Phys.*, **16**, 85 (1976).
5. B. van Leer, 'Towards the ultimate conservative difference scheme. II. Monotonicity and conservation combined in a second order scheme', *J. Comput. Phys.*, **14**, 361 (1974).
6. B. van Leer, 'Towards the ultimate conservative difference scheme. IV. A new approach to numerical convection', *J. Comput. Phys.*, **23**, 276 (1977).

7. B. van Leer, 'Towards the ultimate conservative difference scheme. V. A second order sequel to Godunov's method', *J. Comput. Phys.*, **32**, 101 (1979).
8. A. Harten, 'High resolution schemes for hyperbolic conservation laws', *J. Comput. Phys.*, **49**, 357 (1983).
9. P. K. Sweby, 'High resolution schemes using flux limiter for hyperbolic conservation laws', *SIAM J. Numer. Anal.*, **21**, 995 (1984).
10. P. D. Lax and B. Wendroff, 'Systems of conservation laws', *Commun. Pure Appl. Math.*, **13**, 217 (1960).
11. S. R. Chakravarthy and S. Osher, 'High resolution applications of the Osher upwind scheme for the Euler equations', *AIAA Paper 83-1943*, 1983.
12. P. L. Roe, 'Some contributions to the modelling of discontinuous flows', *Lectures in Applied Mathematics*, Vol. 22, *Proc. 1983 AMS–SIAM Summer Seminar on Large Scale Computing in Fluid Mechanics*, SIAM, Philadelphia, PA, 1985, p. 163.
13. B. P. Leonard, 'Simple high-accuracy resolution programme for convective modelling of continuities', *Int. j. numer. methods fluids*, **8**, 1291 (1988).
14. P. H. Gaskell and A. K. C. Lau, 'Curvature compensated convective transport: SMART, a new boundedness preserving transport algorithm', *Int. j. numer. methods fluids*, **8**, 617 (1988).
15. B. P. Leonard, 'A stable and accurate convective modelling procedure based on quadratic upstream interpolation', *Comput. Methods Appl. Mech. Eng.*, **19**, 59 (1979).
16. P. Tamamidis and D. N. Assanis, 'Evaluation of various high order accuracy schemes with and without flux limiters', *Int. j. numer. methods fluids*, **16**, 931 (1993).
17. F. S. Lien and M. A. Leschziner, 'A general non-orthogonal finite-volume algorithm for turbulent flow at all speeds incorporating second-moment closure, Part 1: Numerical implementation; Part 2: Application', *Comput. Methods Appl. Mech. Eng.*, **114**, 123, 149 (1994).
18. C. G. Speziale, 'On non-linear $k$–$l$ and $k$–$\varepsilon$ models of turbulence', *J. Fluid Mech.*, **178**, 459 (1987).
19. V. Yakhot, S. A. Orszag, S. Thangam, T. B. Gatski and C. G. Speziale, 'Development of turbulence models for shear flows by a double expansion technique', *Phys. Fluids A*, **7**, 1510 (1992).
20. M. M. Gibson and B. E. Launder, 'Ground effects on pressure fluctuations in the atmospheric boundary layer', *J. Fluid Mech.*, **86**, 491 (1978).
21. H. C. Yee, 'Upwnd and symmetric shock-capturing schemes', *NASA TM-89464*, 1987.
22. R. M. Smith and A. G. Hutton, 'The numerical treatment of advection: a performance comparison of current methods', *Numer. Heat Transfer*, **5**, 439 (1982).
23. D. F. Young and F. Y. Tsai, 'Flow characteristics in models of arterial stenosis—I. Steady flow', *J. Biomech.*, **6**, 395 (1973).
24. D. M. Driver and H. L. Seegmiller, 'Features of a reattaching turbulent shear layer', *AIAA Paper 82-1029*, 1982.
25. O. Piccin and D. Cassoudesalle, 'Etude dans la soufflerie F1 des profiles AS239 et AS240', *ONERA Tech. Rep. P.V. 73/1685 AYG*, 1987.
26. F. S. Lien and M. A. Leschziner, 'Approximation of turbulence convection in complex flows with a TVD-MUSCL scheme', *Proc. 5th Int. IAHR Symp. on Refined Flow Modelling and Turbulence Measurement*, Presses de l'ecole nationale de Ponts et chaussées, Paris, 1993.
27. F. S. Lien and M. A. Leschziner, 'Assessment of turbulence-transport models including non-linear RNG eddy-viscosity formulation and second-moment closure for flow over a backward-facing step', *Rep. TFD/93/9*, Department of Mechanical Engineering, UMIST, 1993; *Comput. Fluids*, accepted for publication.
28. F. S. Lien and M. A. Leschziner, 'Modelling 2D and 3D separation from curved surfaces with variants of second-moment closure combined with low-*Re* near-wall formulations', *Proc. 9th Symp. on Turbulent Shear Flows*, Kyoto, 1993.
29. M. W. Wolfshtein, 'The velocity and temperature distribution in one-dimensional flow with turbulence augmentation and pressure gradient', *Int. J. Heat Mass Transfer*, **12**, 301 (1969).